Naval Research Laboratory
Washington, DC 20375-5320

LPD-17 Topside Aerodynamic Study: *FEFLO*

Ravi Ramamurti
William C. Sandberg

Center for Reactive Flow and Dynamical Systems
Laboratory for Computational Physics and Fluid Dynamics

October 10, 2000

20001101 124

DTIC QUALITY INSPECTED 4

REPORT DOCUMENTATION PAGE

Public reporting burden for this collection of information is estimated to average 1 hour per response, including the time for reviewing instructions, searching existing data sources, gathering and maintaining the data needed, and completing and reviewing the collection of information. Send comments regarding this burden estimate or any other aspect of this collection of information, including suggestions for reducing this burden, to Washington Headquarters Services, Directorate for Information Operations and Reports, 1215 Jefferson Davis Highway, Suite 1204, Arlington, VA 22202-4302, and to the Office of Management and Budget, Paperwork Reduction Project (0704-0188), Washington, DC 20503.

1. AGENCY USE ONLY (*Leave Blank*)	2. REPORT DATE	3. REPORT TYPE AND DATES COVERED
	October 10, 2000	NRL Memorandum Report

4. TITLE AND SUBTITLE	5. FUNDING NUMBERS
LPD-17 Topside Aerodynamic Study: *FEFLO*	

6. AUTHOR(S)

Ravi Ramamurti and William C. Sandberg

7. PERFORMING ORGANIZATION NAME(S) AND ADDRESS(ES)	8. PERFORMING ORGANIZATION REPORT NUMBER
Naval Research Laboratory Washington, DC 20375-5320	NRL/MR/6410--00-8498

9. SPONSORING/MONITORING AGENCY NAME(S) AND ADDRESS(ES)	10. SPONSORING/MONITORING AGENCY REPORT NUMBER
Naval Research Laboratory Washington, DC 20375-5320	

11. SUPPLEMENTARY NOTES

12a. DISTRIBUTION/AVAILABILITY STATEMENT	12b. DISTRIBUTION CODE
Approved for public release; distribution is unlimited.	

13. ABSTRACT (*Maximum 200 words*)

The unsteady air flow over the aft deck of the LPD-17 is computed. The primary goal of this project is to demonstrate that a computational capability is available to confidently predict the airwake about ship superstructures. The unstructured mesh-based incompressible flow solver, *FEFLO*, is used to compute this unsteady flow. Computed results are compared with wind tunnel model test experimental data at select locations and shows good agreement. The effects of tunnel walls and heading are studied. The unsteady flow field from the computations can serve as input to the Manned Flight Simulator (MFS) and can also be navigated in a virtual immersive environment in the Grotto at the Naval Research Laboratory.

14. SUBJECT TERMS		15. NUMBER OF PAGES
Airwake Ship superstructure Topside Unsteady flow LPD-17		21
		16. PRICE CODE

17. SECURITY CLASSIFICATION OF REPORT	18. SECURITY CLASSIFICATION OF THIS PAGE	19. SECURITY CLASSIFICATION OF ABSTRACT	20. LIMITATION OF ABSTRACT
UNCLASSIFIED	UNCLASSIFIED	UNCLASSIFIED	UL

CONTENTS

LPD-17 Topside Aerodynamic Study: *FEFLO*

INTRODUCTION

The flow over the landing deck of a ship is inherently unsteady, even if the inflow is perfectly steady. The unsteadiness is due to the complexity of the topside structure which obstructs its smooth passage. This unsteadiness has the potential to adversely affect safe aircraft operations on and in the vicinity of the aft deck. This unsteadiness is further complicated by the hot exhaust gas from the stacks which can create an unfavorable environment for the operation of temperature-sensitive electronics.

The purpose of this study was to validate a computational capability to compute unsteady airwakes due to ship superstructures. The unsteady air flow over the aft deck of the LPD-17 has been computed. The unstructured mesh-based incompressible flow solver, *FEFLO*, was one of the two codes used to compute this unsteady flow. *FEFLO* was validated by comparison of the computed results with experimental wind tunnel data obtained at the Naval Surface Warfare Center, Carderock Division. The computations were performed for two ship headings, 0° and 30°. The unsteady data from the computations will be made available to the Manned Flight Simulator (MFS) at the Naval Air Warfare Center, Paxtuxent River Division.

INCOMPRESSIBLE FLOW SOLVER

FEFLO is a finite element-based incompressible flow solver based on simple, low-order elements. The simple elements enable the flow solver to be as fast as possible reducing the overhead in building element matrices, residual vectors etc. The governing equations are written in Arbitrary Lagrangian Eulerian form which enables simulation of flow with moving bodies. For high Reynolds number flow cases, the mesh requirement is met by employing arbitrary semi-structured grids close to wetted surfaces and wakes. The full details of the flow solver, the rigid body motion and adaptive remeshing are given by Ramamurti et al.[1] and are summarized next.

The governing equations employed are the incompressible Navier-Stokes equations in Arbitrary Lagrangian Eulerian (ALE) formulation. They are written as

$$\frac{Dv}{Dt} + \mathbf{v}_a \cdot \nabla \mathbf{v} + \nabla p = \nabla \cdot \sigma \tag{1a}$$

$$\frac{D\mathbf{v}}{Dt} = \frac{\partial \mathbf{v}}{\partial t} + \mathbf{w} . \nabla \mathbf{v} \tag{1b}$$

$$\nabla \cdot \mathbf{v} = 0 \tag{2}$$

Here p denotes the pressure, $\mathbf{v}_a = \mathbf{v} - \mathbf{w}$, the advective velocity vector (flow velocity $\mathbf{v}$ minus mesh velocity $\mathbf{w}$), and the material derivative is with respect to the mesh velocity $\mathbf{w}$. Both the pressure p and the stress tensor σ have been normalized by the (constant) density ρ, and are discretized in time using an implicit time stepping procedure. It is important for the flow solver to be able to capture the unsteadiness of a flow field. The present flow solver is built as time-accurate from the onset, allowing local timestepping as an option. The resulting expressions are subsequently discretized in space using a Galerkin procedure with linear tetrahedral elements. In order to be as fast as possible, the overhead in building element matrices, residual vectors, etc. should be kept to a minimum. This requirement is met by employing simple, low-order elements that have all the

variables (u,v,w,p) at the same location. The resulting matrix systems are solved iteratively using a preconditioned gradient algorithm (PCG), as described by Martin and Löhner[2]. The flow solver has been successfully evaluated for both 2-D and 3-D, laminar and turbulent flow problems by Ramamurti *et al.*[3,4]

COMPUTATIONAL MODEL

Generation and verification

The first critical and most time-consuming step in this project was the generation of the computational model of the LPD-17 ship that was suitable for computational fluid dynamics. This was achieved by converting the various IGES files of the LPD-17 ship to the grid generation file format of the advancing front grid generator for *FEFLO*. First, GridTool[5] software was employed to translate the IGES files for this ship. Then, the output from GridTool was converted to the format that *FECAD*, the CAD software incorporated within the *FEFLO* software suite, could use, and the entire ship geometry file was assembled. Next, the LPD-17 ship geometry file was trimmed at the water line using GridTool and *FECAD* . The ship configuration was then modified to include the forward and aft masts. A preliminary volume mesh consisting of approximately 300K points suitable for Euler flows was generated. Next, the configuration was modified by adding the "Stumpy V" masts. Other features that were added after examination of the wind-tunnel physical model included the bulwark around the bow and all the deck areas. The computational representation of the wind-tunnel model was compared to that of the experiment at several locations along the length of the ship. Figure 1 shows the comparison of the model at $x = 10$m, and the agreement is good.

0° heading

A grid consisting of 360,732 points and 1,987,470 tetrahedral elements was generated for this configuration. This surface triangulation was also provided as the input geometry specification for use with the FAST3D code. The flow past this configuration was obtained in 4500 time steps using *FEFLO* . The flow quantities at several locations, where experimental data are collected, were computed. Although these were instantaneous values at one time instant, these computational results were provided to the experimentalists to give them an idea for the resolution required for data acquisition. The computational model at that time lacked several features that were present in the wind tunnel model. These are shown in Figs. 2a-c. The modifications required included several radar domes, gun-mounts, antennae, exhaust stacks and cat-walks along the deck. These features were added and the computational model was also placed in the exact wind tunnel configuration. The coordinate system orientation and the velocity component directions are also shown in Fig. 2c. A grid consisting of 420,341 points and 2,316,922 tetrahedral elements was generated for this configuration. The unsteady flow over this configuration at 0° heading and at an inflow velocity of 30 knots was computed for approximately 4 seconds. The velocities and pressure at several locations in the landing deck region were averaged in time. The comparison of the velocities is shown in Fig. 3. It can be seen that the longitudinal (u-velocity) and the normal (w-velocity) components exhibit a symmetric variation, while the transverse (v-velocity) component exhibits an anti-symmetric variation. This is expected as the location is aft of the ship in the wake. The comparison with the experimental results is good. In Fig. 3a, the difference in the u-velocity component near the centerline is due to the fact that in the experiments there is a data dropout when the velocity magnitude is below 15 knots. This results in a higher average velocity being indicated for such locations in the experimental values. The comparison of the velocities at the aft-landing spot is shown in Fig. 4. Again, the comparison is reasonable, except near the centerline for the u-velocity component. Figure 5 shows the variation of the velocity components along the centerline

of the deck. Here, the x - coordinate is relative to the forward landing spot. From Fig. 5a, it can be seen that a recirculation region is present from $x = -50$ft up to $x = -20$ft, approximately. The trends in the computations are similar to that of the experiments, except that the magnitude is lower for the u-component, and is higher for the w-component of velocity, in the present study. This discrepancy in the u and w component of the velocity may be due to the drop-outs of low magnitude velocity in the experiments, which are expected in a recirculation zone, and/or due to the blockage effect of the probe traverse mechanism. Both of these possibilities could lead to a higher u-component (longitudinal) experimentally, while reducing the w-component (normal) of velocity. Figure 6 shows the pressure variation at the two probe locations and along the centerline of the deck. There were no pressure measurements for comparison. In this figure, the pressure is non-dimensionalized with respect to the free-stream pressure. The variation is symmetric in the wake, Fig. 6a, and is nearly symmetric in the deck region at the aft-landing spot, Fig. 6b. Figure 7 shows the surface definition and triangulation of the computational model. Figures 8a-d show the results of the computations at one instant of time, $t = 3.139$ sec. In this figure all the quantities are non-dimensional and are normalized with respect to the free stream values. At this instant, there is a large recirculation region behind the aft-mast and in the landing deck region, between the hangar and the forward landing spot, as shown in Figs. 8b-d. It is interesting to note in Figs. 8b and c, the instantaneous high velocity gradient which exists just off the deck near the transom.

Comparison of station data time histories

Velocity time histories were also obtained at several points in a box-like grid in the deck area. These points correspond to the 279 stations where measurements were obtained. The experimental measurements were obtained at longitudinal locations of $x = 153.5$, 170.0, 188.0, 202.0, 210.0, 220.0 and 240.0 m, at lateral locations of $y = 0$, ± 6, ± 12, ± 18 and ± 24m, and at vertical location of $z = 19$, 24, 29, 34 and 44m. Because of the presence of the flight deck at $z = 19$m, measurements were not taken forward of $x = 210$m location. Unsteady data of velocity and pressure were computed at these 279 locations for approximately 8 seconds. Figures 9-11 show the time history of the velocity components at three locations, and the comparison with experimental data. From Fig. 9, it is clear that the computed velocity magnitudes and trends agree well with the experiments. Figure 9a shows that the longitudinal component exhibits large excursions, approximately 25ft/s in 0.2sec, at t=3.8sec. The computed values of the longitudinal velocity along the centerline at the aft-landing spot, $x = 188.0$m, $z = 34$m, shown in Fig. 10a, are lower compared to the experiments. The reason for this was described previously. In all the time histories, the experimental data exhibit a much higher frequency content than is obtained from the *FEFLO* computations. Figures 10a and 11a are important to note, in this regard, since the computed low frequency behavior at the forward landing spot may be important to helicopter operations. A Fourier transform of the computed data at these three locations was performed for the last 4.0 seconds of simulation. The amplitude of the various frequency components of velocity are shown in Figs. 12a-c. From Fig. 12a, one notices that there is considerably more intensity in the low frequency components on the centerline than off the centerline. This is an indication of the longitudinal velocity variations existing in the recirculation zone behind the hangar. For all the components of velocity, the amplitude of fluctuation diminishes as frequency is increased and is negligible for frequencies greater than 50 *Hz*, as expected. From Fig. 12b, it can be seen that the amplitude reaches a maximum at about 11*Hz* and drops thereafter. The magnitude of the fluctuation drops for $x = 240$m and $y = 24$m, as this location is not directly behind the hangar and the ship superstructure.

Effect of tunnel walls

Next, the effect of the proximity of the tunnel walls to the model was computationally studied. For this investigation, the tunnel width was increased from approximately 124" to 150", the height increased from 48" to 60", and the downstream boundary moved from 272" to 406". The tunnel dimensions are for the 1/94th scale model. The effect of moving the tunnel walls is shown in Figs. 13 and 14, and is observed to be minimal.

30° heading

The effect of ship heading on airwake was studied next. Figure 15 shows the computational model in the wind tunnel, with a ship heading of 30° to port. The results of the computation are shown in Fig. 16. It can be seen that there is a larger variation of pressure across the landing deck region and clear formation of a Karman vortex street downstream of the ship. At $x = 188$m and z =44m, the fluctuations in the velocity components are decreased considerably for the 30° heading. This is because of the fact that in the 0° heading this location is in the wake of the aft-mast and as the heading is changed, it is outside the wake of the flow past the aft-mast. The mean of the longitudinal component is increased from 34.0ft/s to 61.7ft/s. The mean of the normal component is increased from –3.5ft/s to +3.8ft/s, indicating that this location is out of the recirculation region as the heading is increased and experiences an increase in the upward component of the flow. Figure 17c shows that the fluctuation in the transverse component are nearly symmetric for the 0° heading and magnitude of the amplitude of fluctuation is reduced from 8.0ft/s to 3.0ft/s. This is as one would expect since now the transverse flow is predominantly to port at this location for the 30° case and oscillates about zero with a lower magnitude for the 0° case. At a lower elevation from the deck level, $z = 24.0$m, the magnitude of the fluctuations are in the same range for both the headings studied, as can be seen from Fig. 18. The reason is that the location is only 5m above the deck level and is therefore in the wake of the flow over the hangar. One expects, and we observe, larger transverse oscillation magnitudes at this lower elevation.

CONCLUSIONS AND FUTURE WORK

The incompressible flow solver *FEFLO* was used to compute the unsteady airwake of the LPD-17. Comparison with wind tunnel model test experimental data at select locations showed good agreement. The primary goal of this project was to demonstrate that a computational capability is available to confidently predict the airwake about ship superstructures. The good comparison with measured data is evidence that the goal has been accomplished.

The unsteady time history data was saved at 279 points, corresponding to the experimental observation locations. This data is available for future analysis, beyond what has been reported here. Computations indicate a lower frequency and lower magnitude velocity field at the forward landing location than is found from the experimental data. This difference is attributed to data dropouts and hence the computational results are considered more representative of the actual velocity field. The effect of tunnel walls and heading were studied. An FFT analysis of the unsteady flow velocities was conducted and showed that the amplitude of fluctuations in all the velocity components were insignificant after $50Hz$ and the fluctuations in the normal velocity near the aft-landing spot reached a maximum around $11Hz$. These spectra will next be compared with the experimental data. A finer grid solution for the 0° heading is being performed and the time history and spectra will be compared to assess the sensitivity of the grid and time-step refinement. The unsteady flow field from the computations can serve as input to the Manned Flight Simulator (MFS) and can also be navigated in a virtual immersive environment in the Grotto at the Naval Research Laboratory.

ACKNOWLEDGEMENTS

REFERENCES

1. Ramamurti, R., Sandberg, W.C. and Löhner, R., "Simlation of a Torpedo Launch Using a 3-D Incompressible Finite Element Flow Solver and Adaptive Remeshing," AIAA Paper No. 95-0086, January 1995.

2. Martin, D. and Löhner, R., "An Implicit Linelet-Based Solver for Incompressible Flows," *AIAA Paper* No. 92-0668, 1992.

3. Ramamurti, R. and Löhner, R., "Evaluation of an Incompressible Flow Solver Based on Simple Elements," *Advances in Finite Element Analysis in Fluid Dynamics*, 1992, FED Vol. 137, Editors: M.N Dhaubhadel et al., ASME Publication, New York, pp. 33-42.

4. Ramamurti, R., Löhner, R. and Sandberg, W.C., "Evaluation of Scalable 3-D Incompressible Finite Element Solver," *AIAA Paper* No. 94-0756, 1994.

5. Samareh, J., "GridTool: A surface Modeling and Grid Generation Tool," Proc. of the workshop on Surface Modeling, Grid Generation, and Related Issues in CFD Solutions, NASA CP-3291, May 1995.
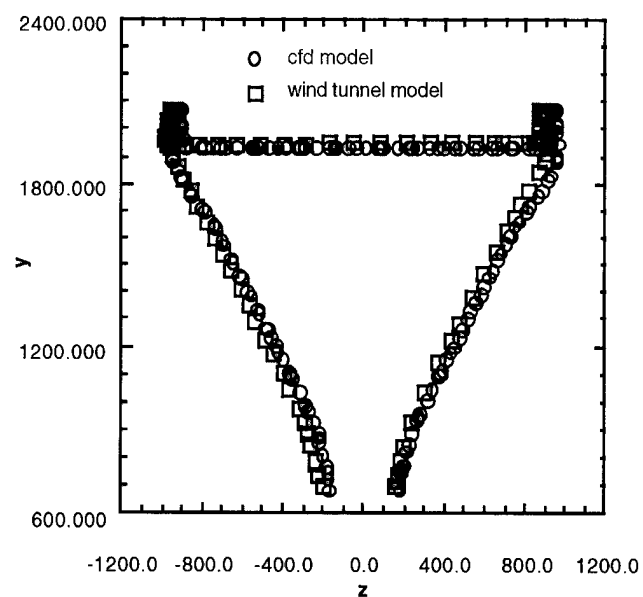
Figure 1. Comparison of the Geometry at $x = 10$m
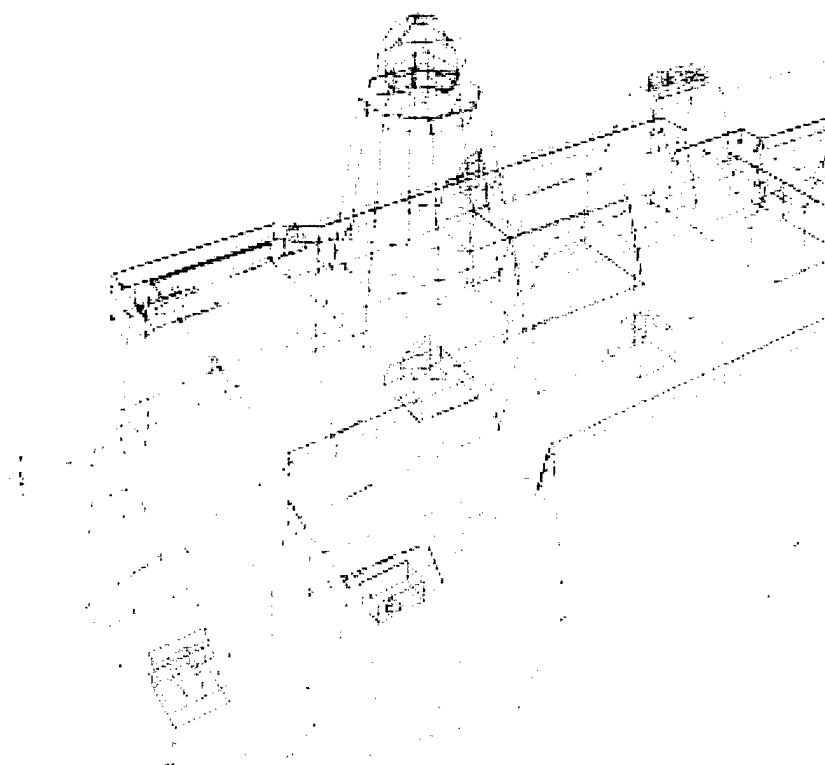
a.   Front Mast region

Figure 2. Modifications to the LPD-17 configuration
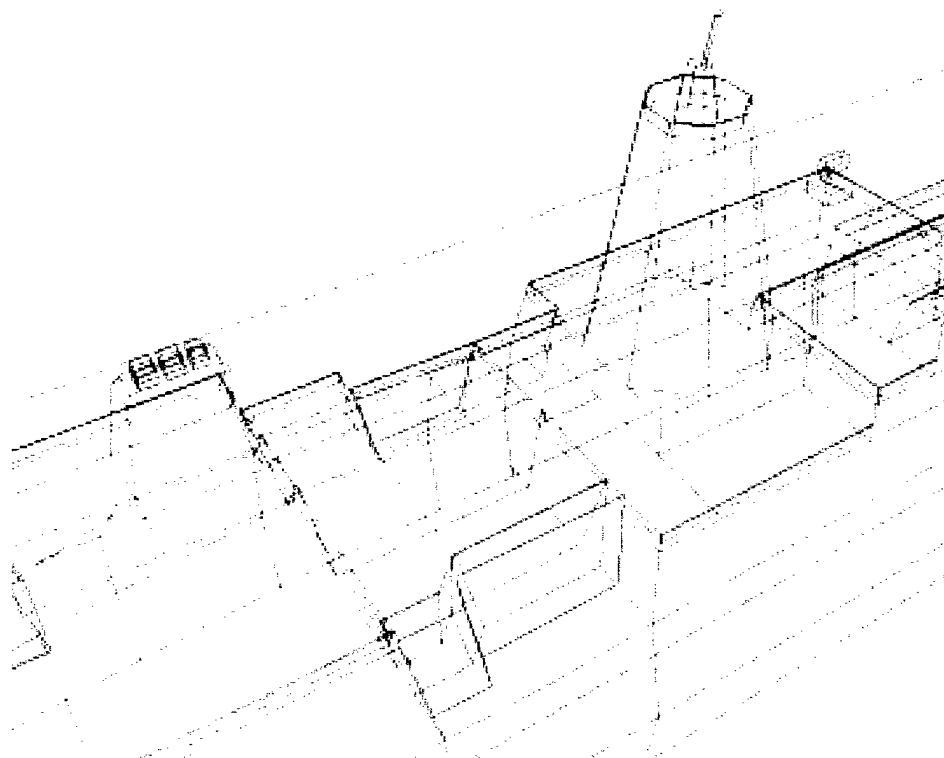
b. aft Mast region
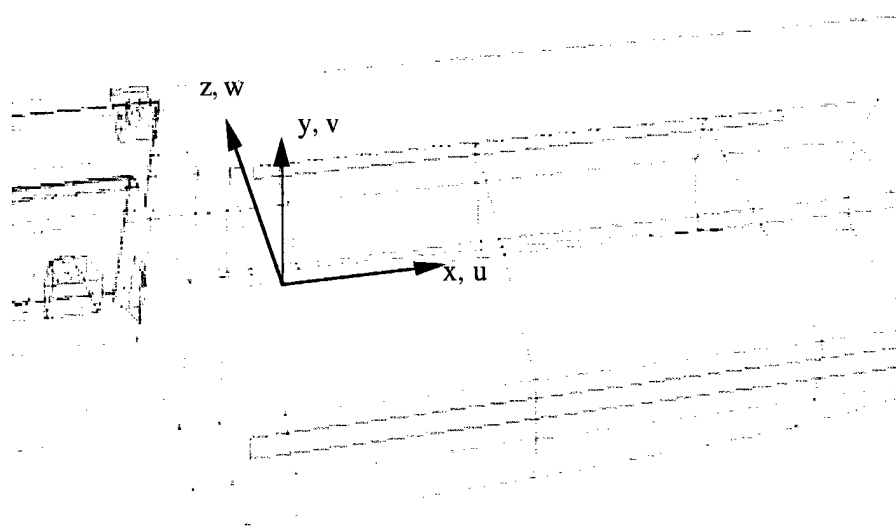
c. Landing deck region

Figure 3. Modifications to the LPD-17 configuration
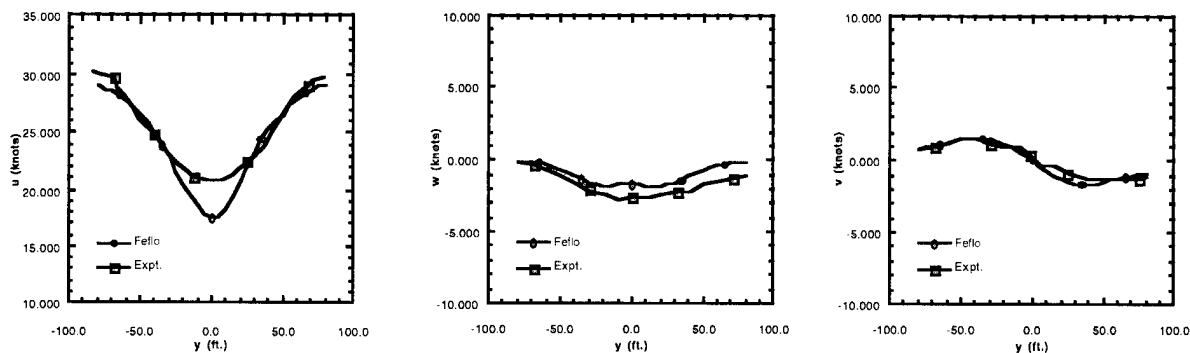
a. u-velocity vs. y   b. w-velocity vs. y   c. v-velocity vs y

Figure 4. Variation of velocity at 300 ft behind forward landing spot, z = 20ft, 0° heading
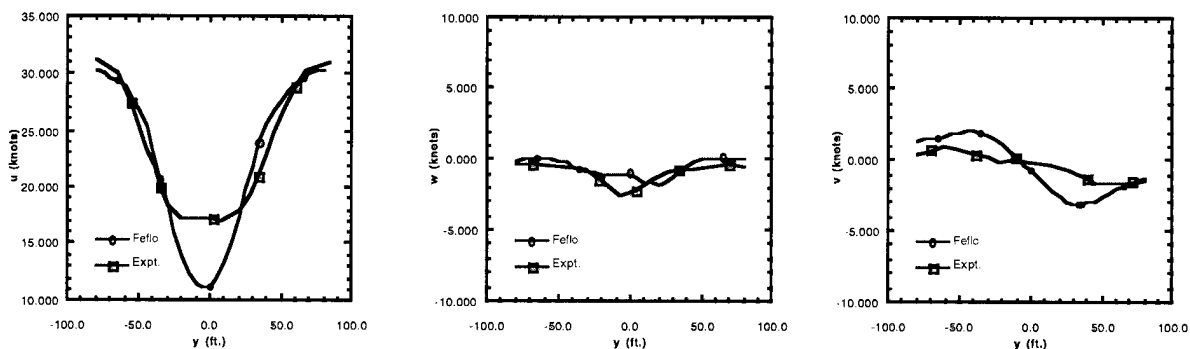
a. u-velocity vs. y   b. w-velocity vs. y   c. v-velocity vs y

Figure 5. Variation of velocity at aft-landing spot, z = 20ft, 0° heading
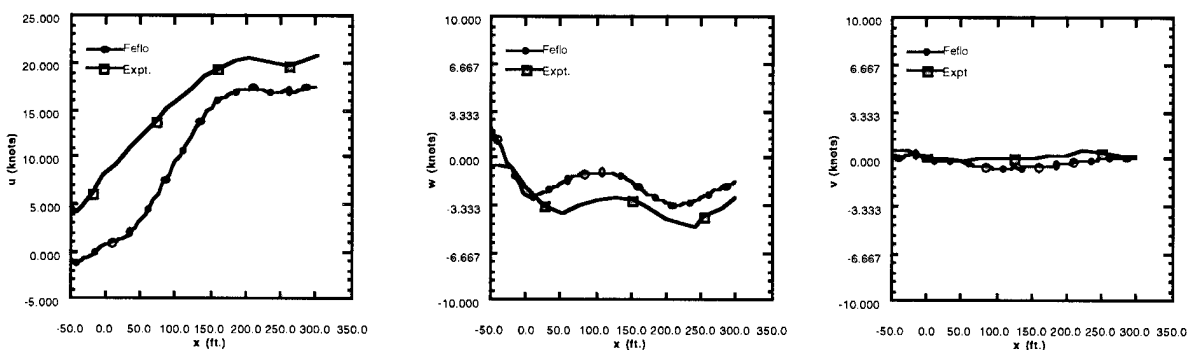
a. u-velocity vs. x   b. w-velocity vs. x   c. v-velocity vs x

Figure 6. Variation of velocity along the centerline of the deck, z = 20ft, 0° heading
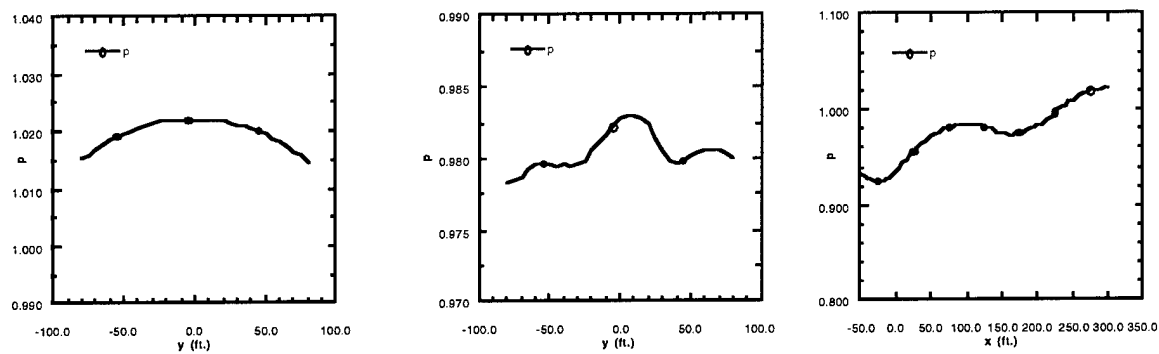
a. 300ft behind forward landing spot   b. aft-landing spot   c. centerline

Figure 7. Variation of pressure, z = 20ft, 0° heading
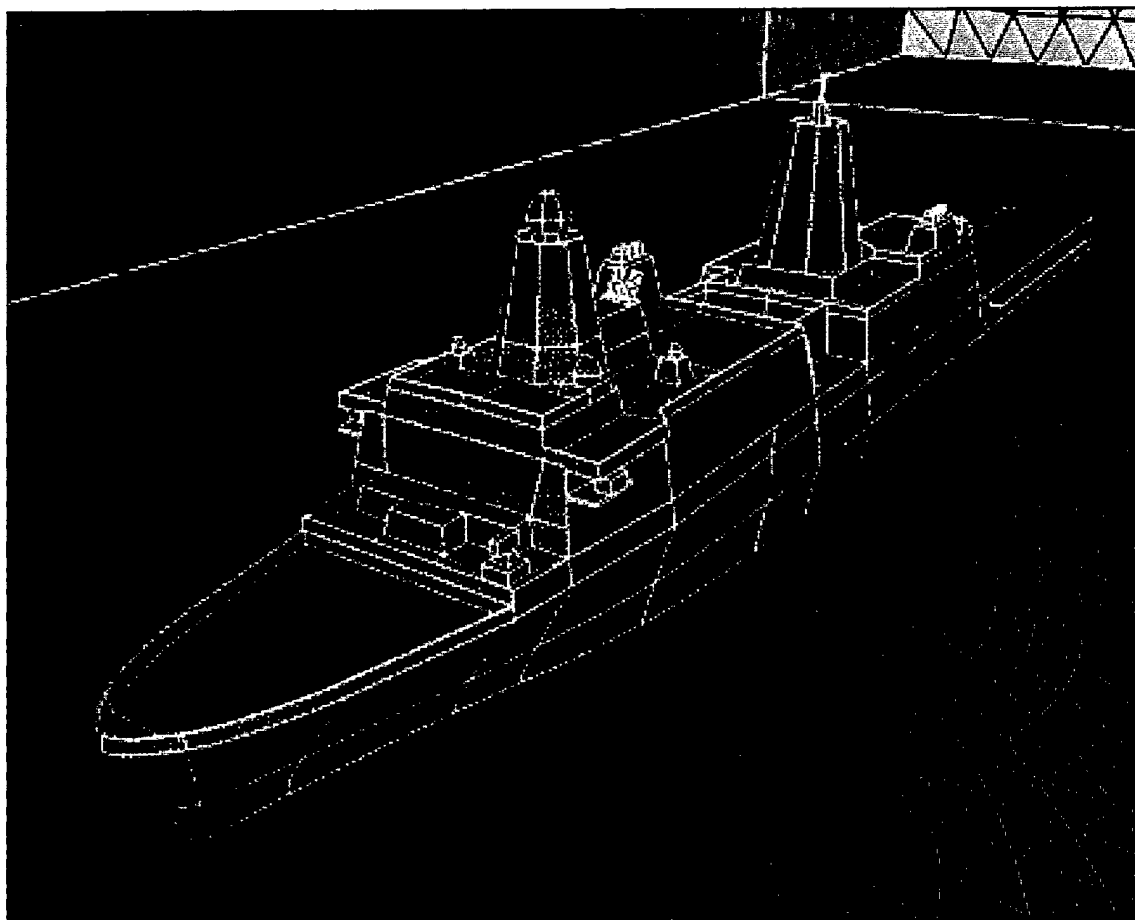
Figure 8. Surface Definition of the LPD-17 configuration, 0° heading
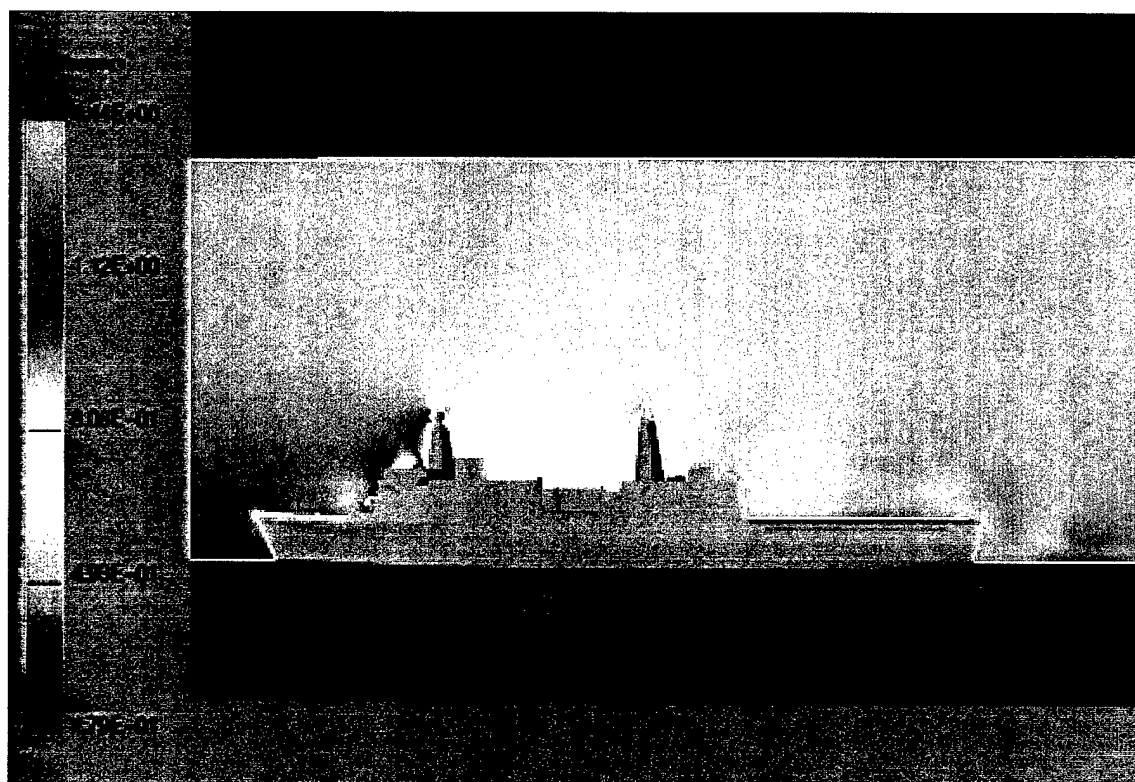
a. Pressure, y=0
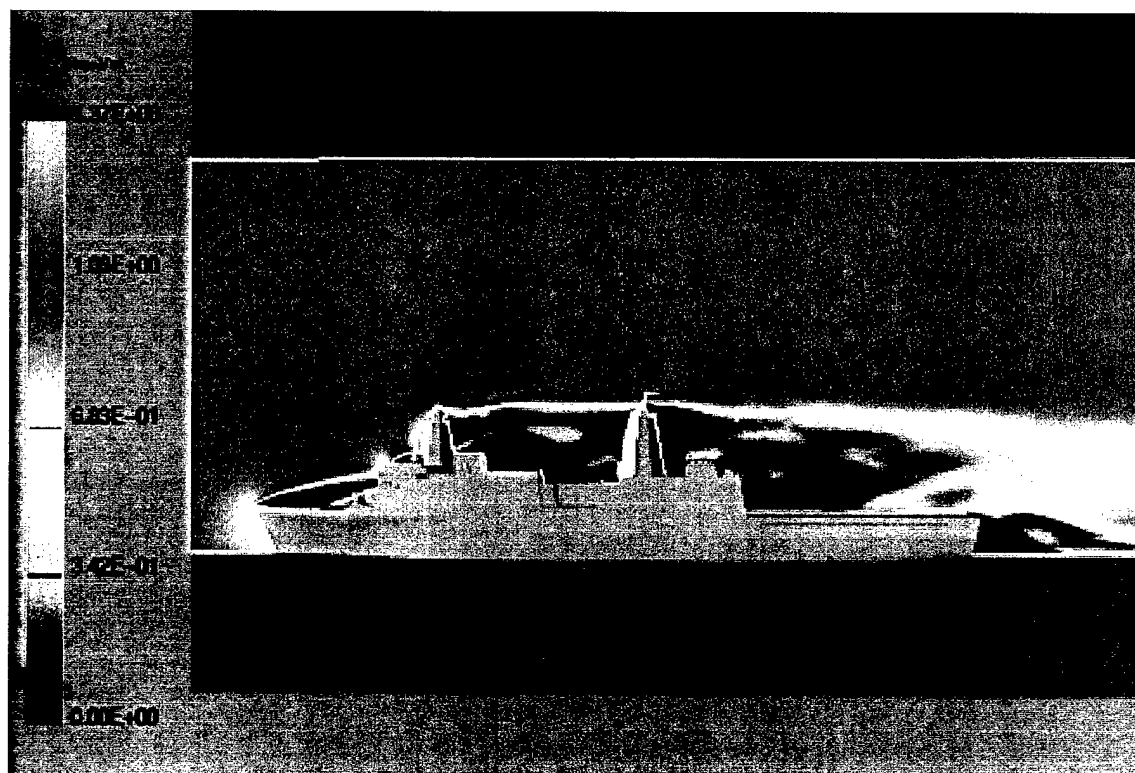
b. Absolute Velocity, y=0

Figure 9. Results of flow past LPD-17 configuration, 0° heading, t= 3.139 Sec.
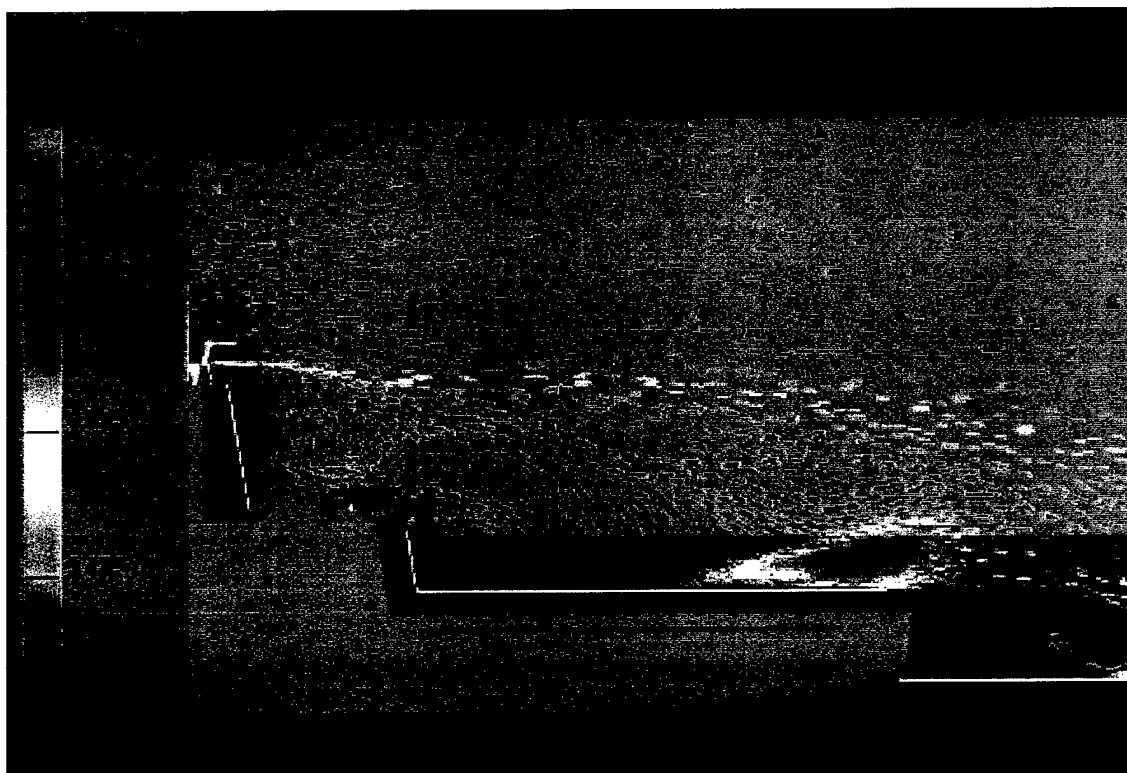
c. Velocity Vectors, y=0
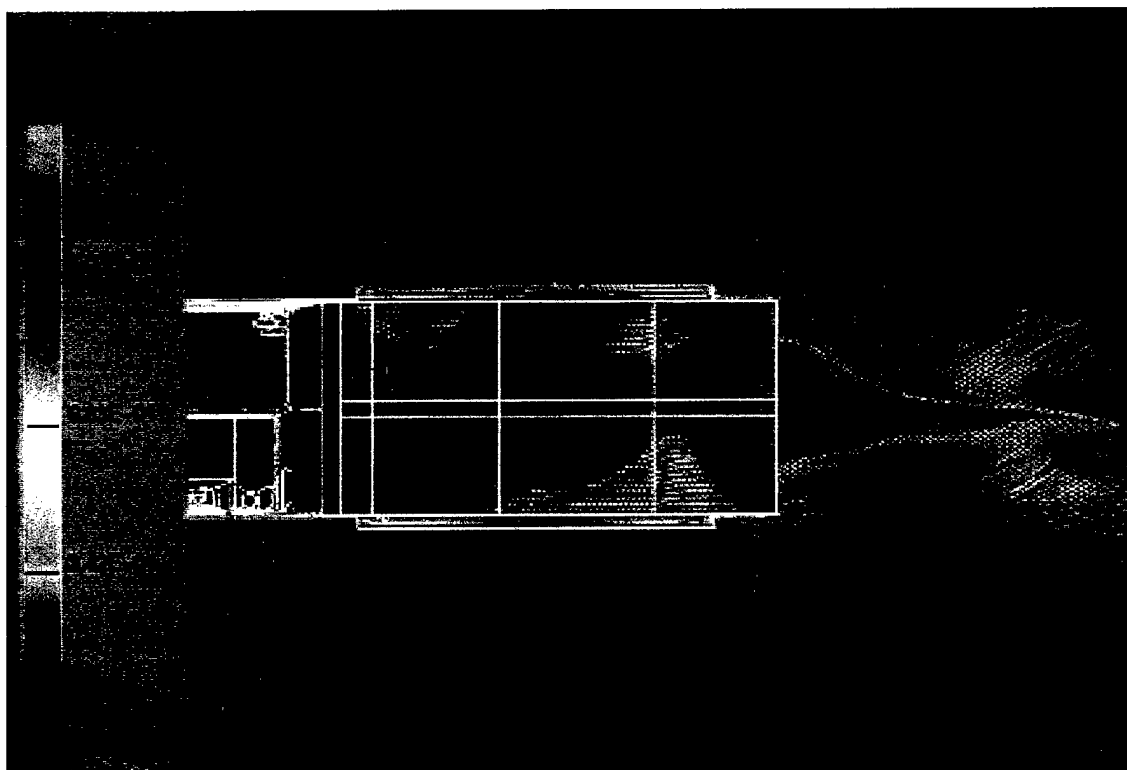
d. Velocity vectors on the surface

Figure 10. Results of flow past LPD-17 configuration, 0° heading, t= 3.139 Sec.
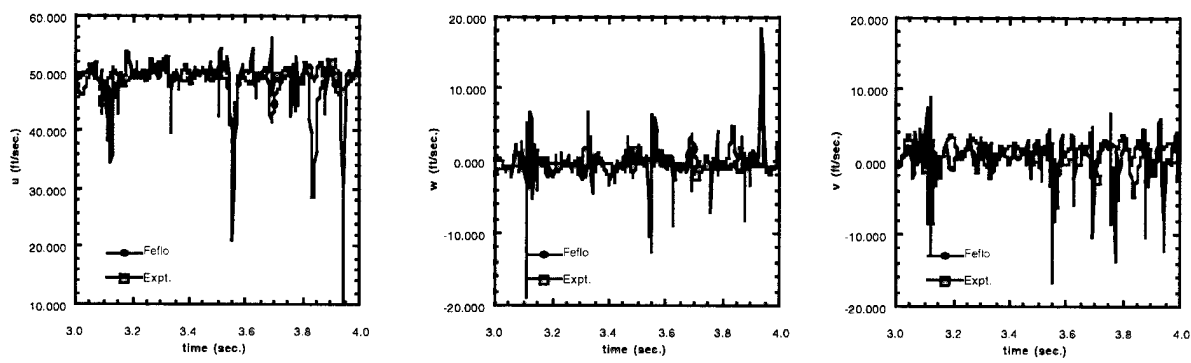
a. longitudinal   b. vertical   c. transverse

Figure 11. Time history of Velocity, x = 240m, y = -24m, z = 19m, 0° heading
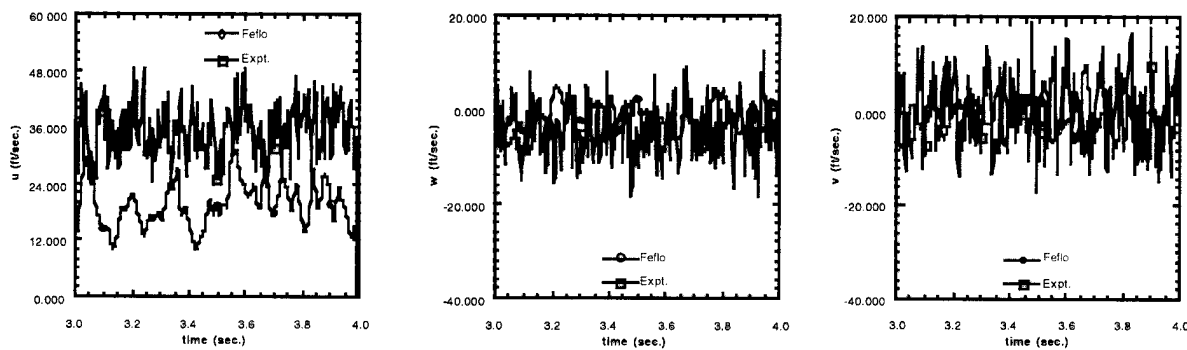
a. longitudinal   b. vertical   c. transverse

Figure 12. Time history of Velocity, x = 188m, y = 0, z = 34m, 0° heading
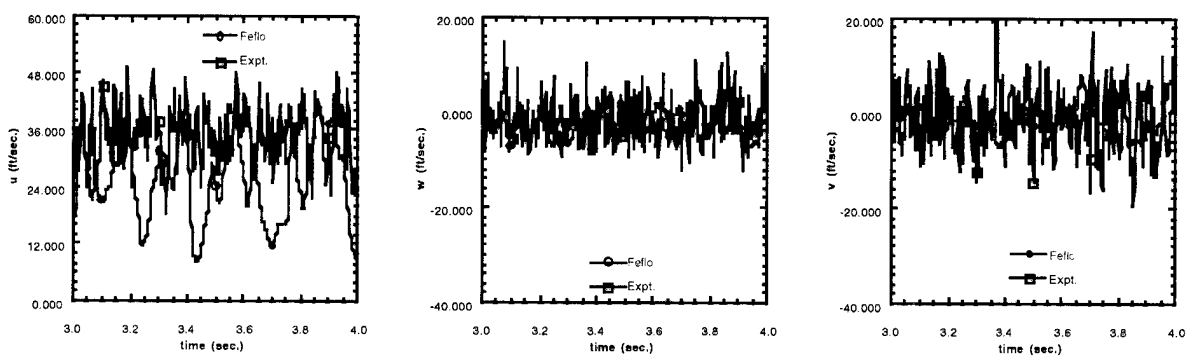
a. longitudinal   b. vertical   c. transverse

Figure 13. Time history of Velocity, x = 188m, y = 6m, z = 34m, 0° heading
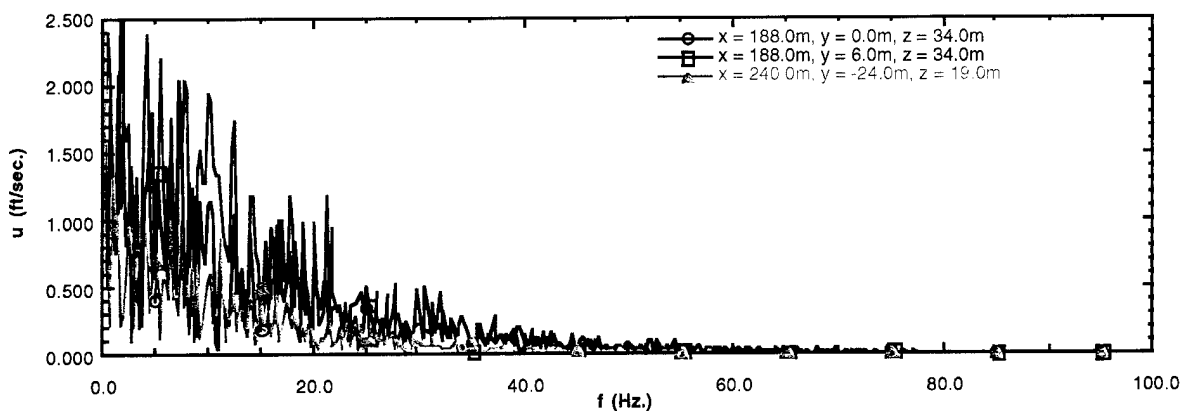
a. amplitude of longitudinal component
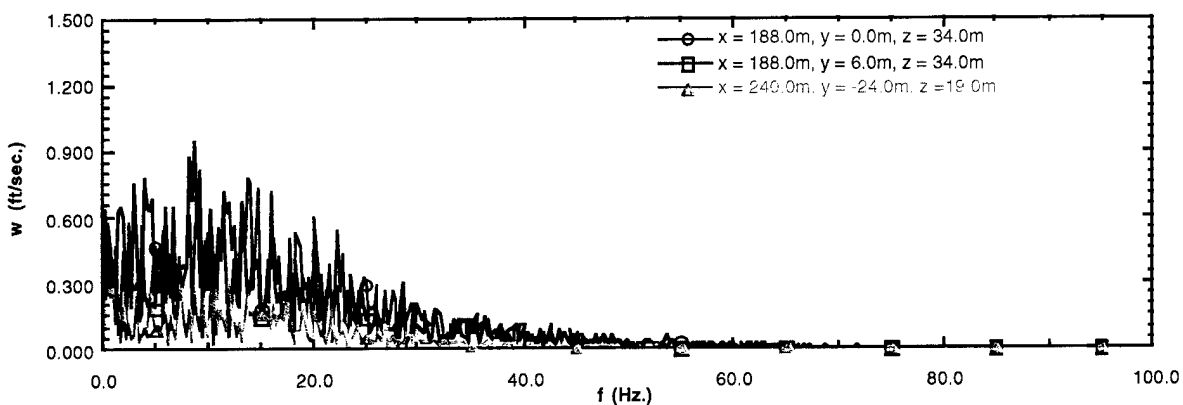
b. amplitude of vertical component
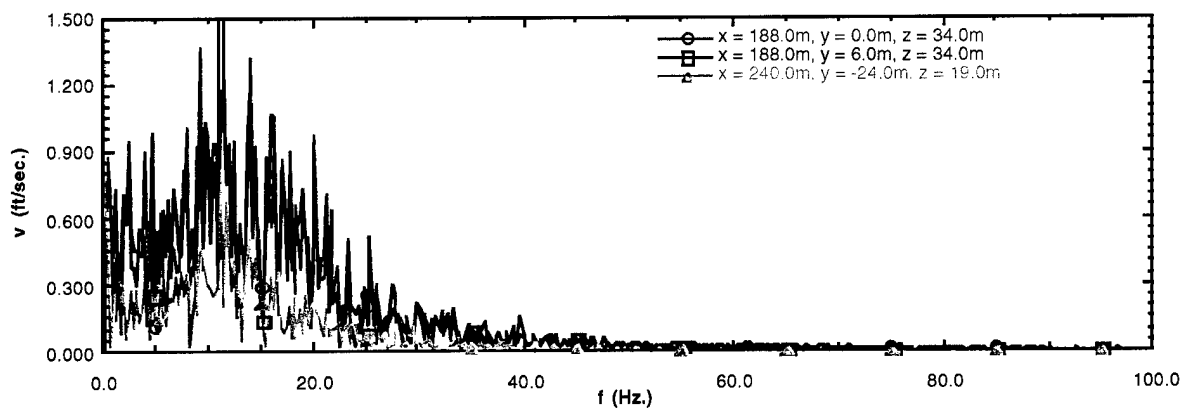
c. amplitude of transverse component

Figure 14. Fourier components of velocity
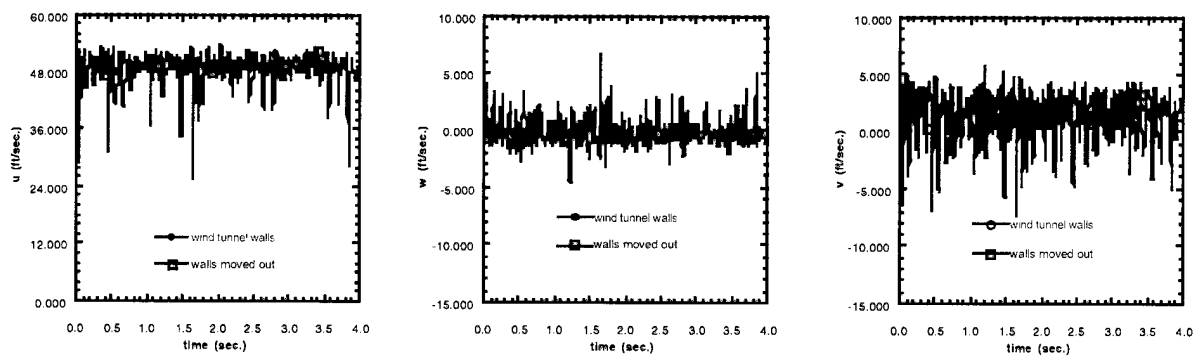
a. longitudinal   b. vertical   c. transverse

Figure 15. Effect of Tunnel Walls, x = 240.0m, y = -24.0m, z=19.0m, 0° heading
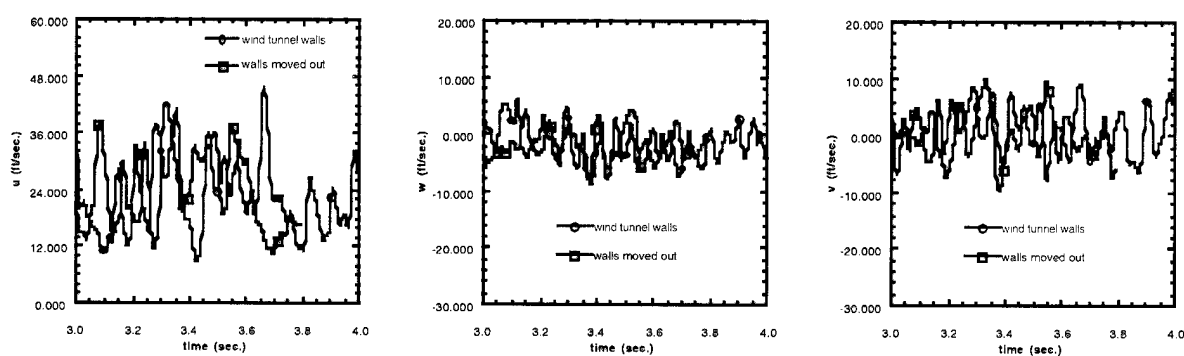
a. longitudinal   b. vertical   c. transverse

Figure 16. Effect of Tunnel Walls, x = 188.0m, y = -6.0m, z=34.0m, 0° heading
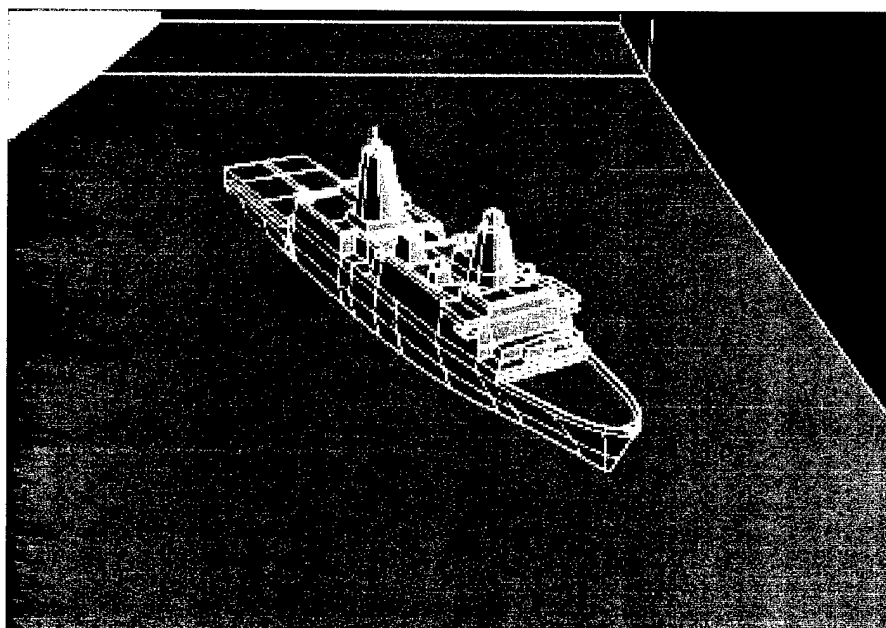
Figure 17. Surface Definition of LPD-17, 30° heading
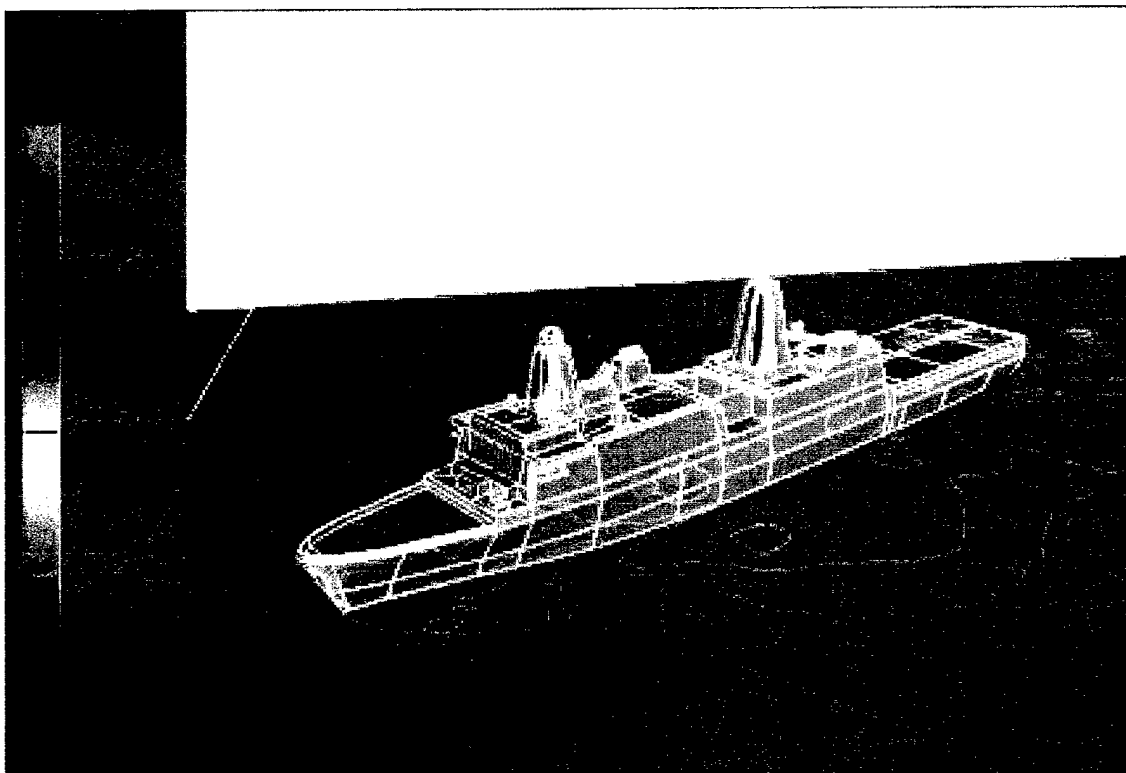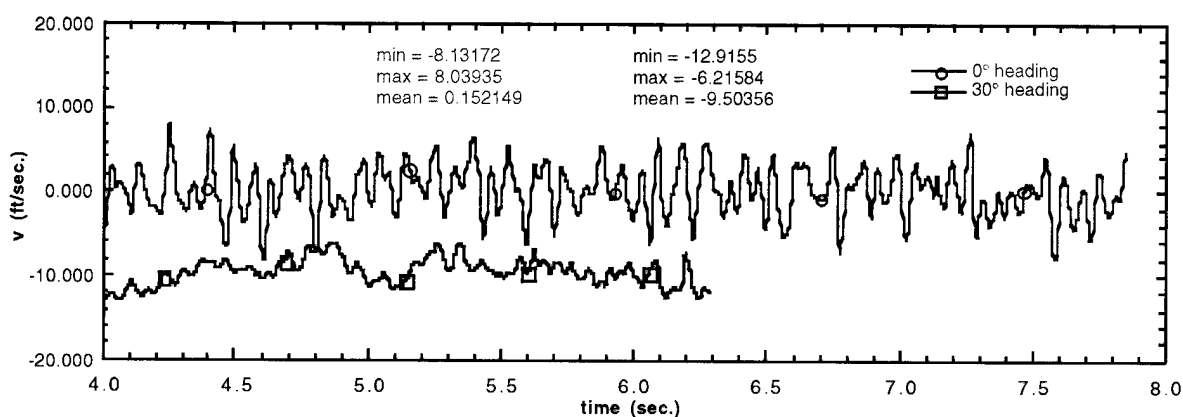
a. Pressure
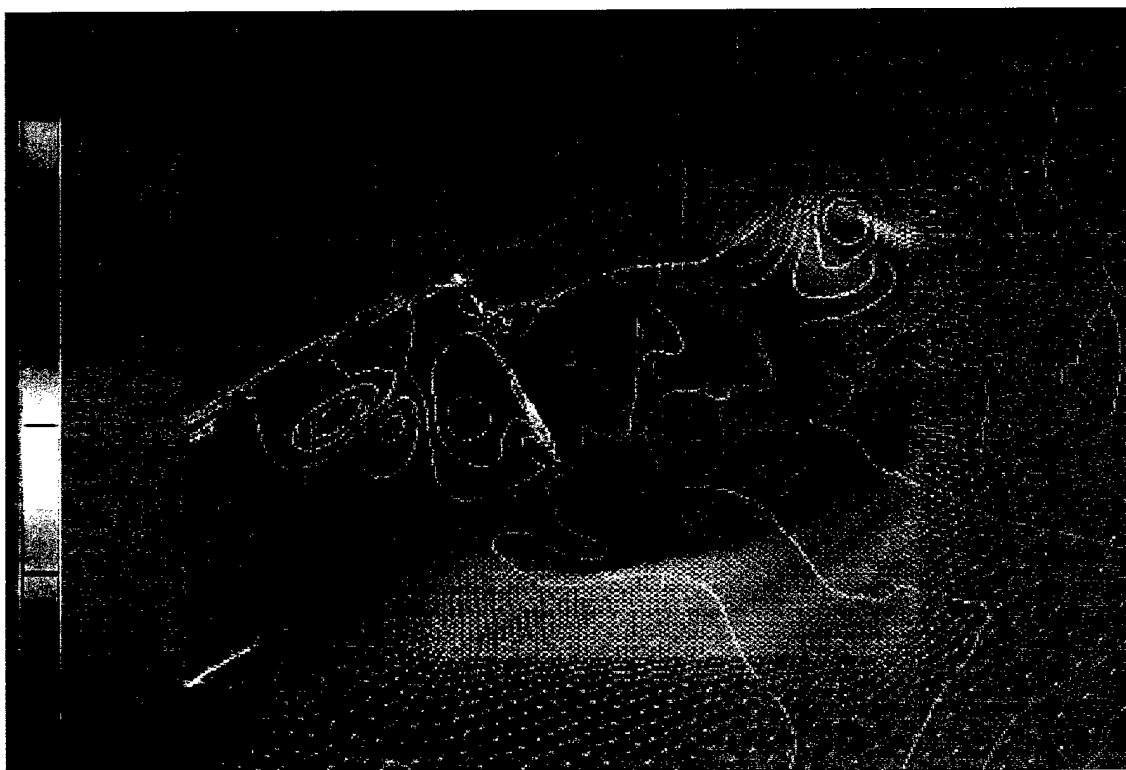
b. Velocity Vectors

Figure 18. Flow Past LPD-17 configuration, 30° heading, t= 3.139 Sec.
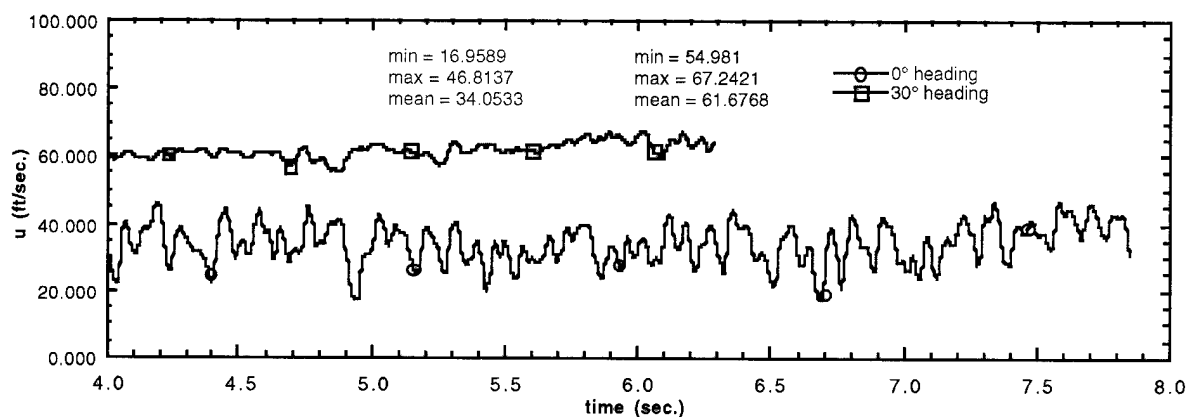
a. Longitudinal velocity
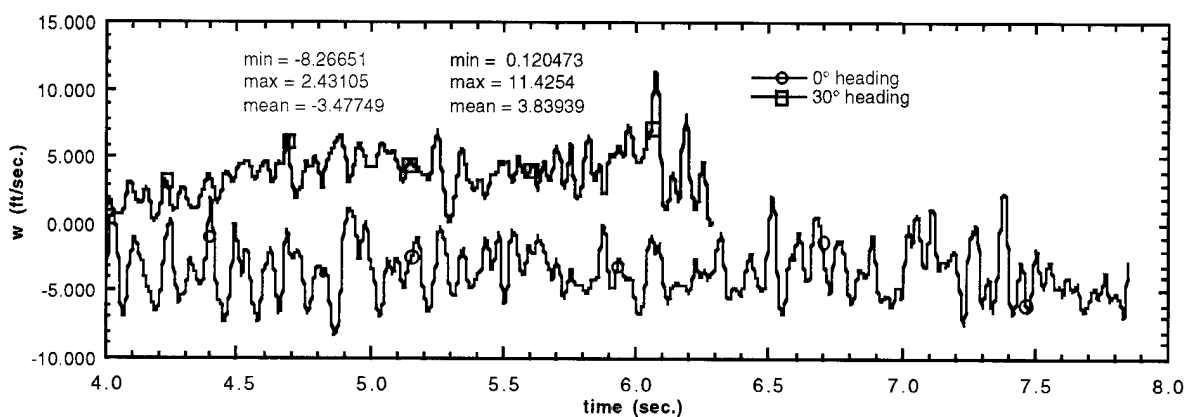
b. Vertical velocity
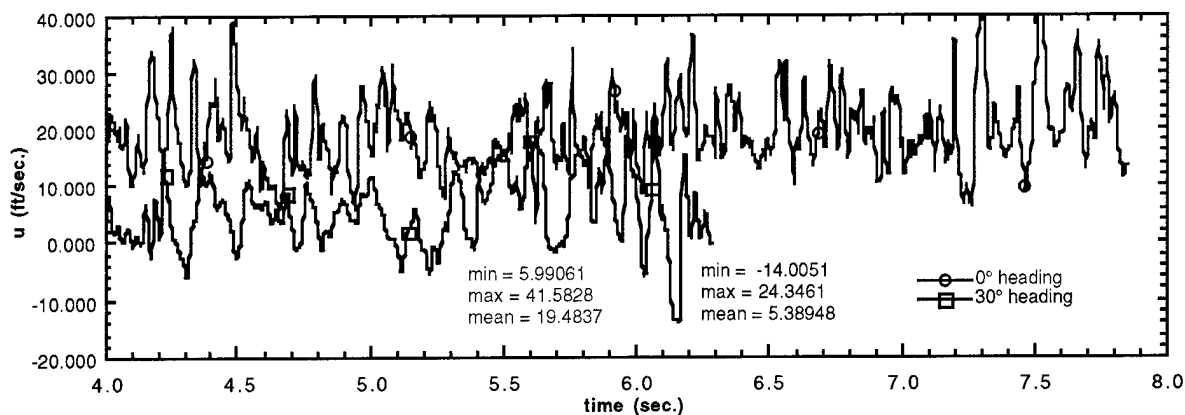

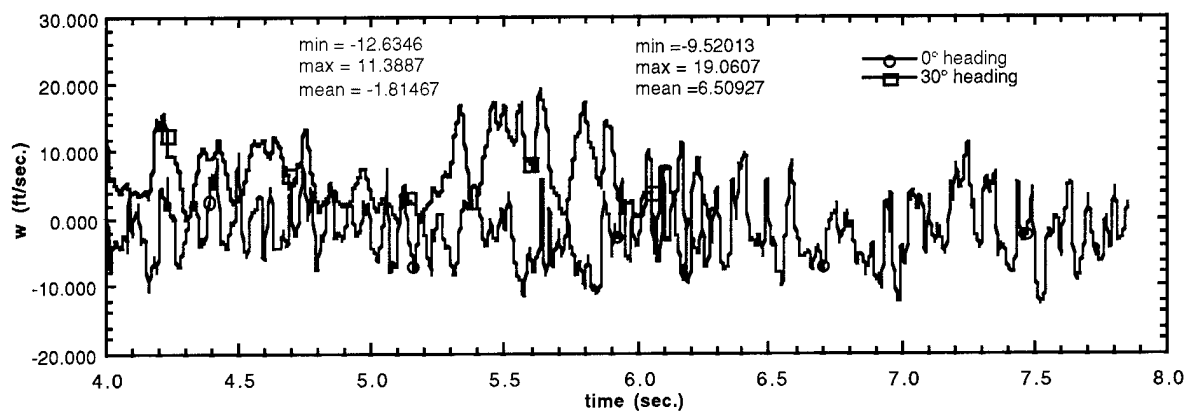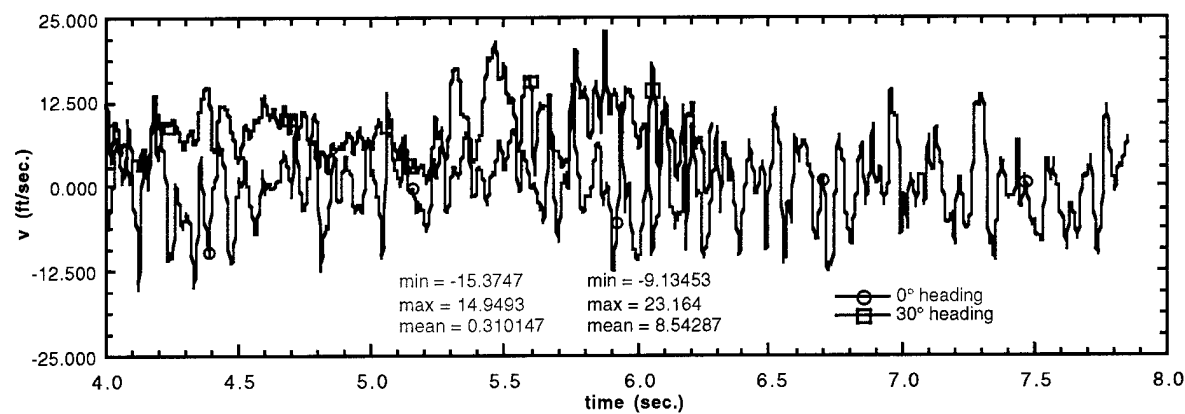c. Transverse velocity

Figure 19. Effect of Heading, x = 188.0m, y = 0m, z=44.0m

a. Longitudinal velocity

b. Vertical velocity

c. Transverse velocity

Figure 20. Effect of Heading, x = 188.0m, y = 0m, z=24.0m